



HAL
open science

cGAS-STING is responsible for aging of telomerase deficient zebrafish.

Naz Serifoglu, Giulia Allavena, Bruno Bastos-Lopes, Marta Marzullo, Pavlos Bousounis, Eirini Trompouki, Miguel Godinho Ferreira

► **To cite this version:**

Naz Serifoglu, Giulia Allavena, Bruno Bastos-Lopes, Marta Marzullo, Pavlos Bousounis, et al.. cGAS-STING is responsible for aging of telomerase deficient zebrafish.. 2024. hal-04502630

HAL Id: hal-04502630

<https://hal.science/hal-04502630>

Preprint submitted on 13 Mar 2024

HAL is a multi-disciplinary open access archive for the deposit and dissemination of scientific research documents, whether they are published or not. The documents may come from teaching and research institutions in France or abroad, or from public or private research centers.

L'archive ouverte pluridisciplinaire **HAL**, est destinée au dépôt et à la diffusion de documents scientifiques de niveau recherche, publiés ou non, émanant des établissements d'enseignement et de recherche français ou étrangers, des laboratoires publics ou privés.

1 **cGAS-STING is responsible for aging of telomerase deficient zebrafish.**

2

3 Naz Şerifoğlu¹, Giulia Allavena¹, Bruno Bastos-Lopes¹, Marta Marzullo^{2,*}, Pavlos
4 Bousounis^{3,4}, Eirini Trompouki¹ and Miguel Godinho Ferreira¹

5

6 1- Institute for Research on Cancer and Aging of Nice (IRCAN), CNRS UMR7284,
7 INSERM U1081, Université Cote d'Azur, 06107 Nice, France.

8 2- Instituto Gulbenkian de Ciência, Oeiras, Portugal

9 3- Department of Cellular and Molecular Immunology, Max Planck Institute of
10 Immunobiology and Epigenetics, Freiburg, Germany

11 4- Faculty of Biology, University of Freiburg, Freiburg, Germany

12

13 *current address: Department of Biology and Biotechnologies, Sapienza University of
14 Rome, Rome, Italy.

15

16

17

18

19

20

21

22

23

24

25

26

27

28

29

30 Corresponding Author: Miguel-Godinho.FERREIRA@unice.fr

31

32

33 **Keywords:** Telomerase, cGAS-STING, inflammation, aging, zebrafish

34

35 **Abstract (1088 characters/151 words)**

36 Telomere shortening occurs in multiple tissues throughout aging. When telomeres
37 become critically short, they trigger DNA damage responses and p53 stabilization, leading
38 to apoptosis or replicative senescence. *In vitro*, cells with short telomeres activate the
39 cGAS-STING innate immune pathway resulting in type I interferon inflammation and
40 senescence. However, the consequences of these events to the organism are not yet
41 understood. Here, we show that *sting* is responsible for premature aging of telomerase-
42 deficient zebrafish. We generated *sting*^{-/-} *tert*^{-/-} double mutants and observed a thorough
43 rescue of *tert*^{-/-} phenotypes. At the cellular level, lack of cGAS-STING in *tert* mutants
44 resulted in reduced senescence, increased cell proliferation, and low inflammation despite
45 similar short telomeres. Critically, absence of *sting* function resulted in dampening of the
46 DNA damage response and low p53 levels. At the organism level, *sting*^{-/-} *tert*^{-/-} zebrafish
47 regained fertility, delayed cachexia, and cancer incidence, resulting in increased
48 healthspan and lifespan of telomerase mutants.

49

50

51 **Introduction (3612 characters /489 words)**

52 Telomerase deficiency in humans results in the development of telomere biology
53 disorders (TBDs) that include idiopathic pulmonary fibrosis, dyskeratosis congenita and
54 aplastic anemia¹. Common aspects of TBDs relate to accelerated telomere shortening,
55 loss of tissue regeneration, premature aging phenotypes and shorter life span^{2,3}. Zebrafish
56 possess human-like telomere lengths that shorten to critical lengths during their lifetime.
57 Like human TBDs, telomerase-deficient zebrafish (*tert*^{-/-}) have accelerated telomere
58 shortening, low cell proliferation, tissue damage, and reduced lifespan⁴⁻⁶. *tert*^{-/-} zebrafish
59 also develop chronic inflammation, increased infections, and accelerated incidence of
60 cancer^{7,8}. Like in humans⁹, we have recently shown that not all organs age at the same
61 rate⁸. The zebrafish intestine becomes dysfunctional earlier and triggers systemic aging.
62 Reduced proliferation of intestine cells results in loss of tissue integrity, microbiota
63 dysbiosis and systemic inflammation⁸.

64 Type I interferon response and secretion of pro-inflammatory cytokines through
65 activation of cGAS-STING is triggered by DNA damage, including telomeric damage,
66 leading to the formation of micronuclei (MN)¹⁰⁻¹³. The cytosolic DNA sensor, cGAS
67 (cGMP-AMP synthase), becomes activated upon binding to double-stranded DNA,
68 encompassing both microbial and self-DNA¹⁴. Upon recognition of cytosolic DNA, cGAS
69 initiates the production of the second messenger cGAMP that binds and activates the

70 adaptor protein STING^{15,16}. Subsequently, STING recruits TBK1 (TANK-binding kinase 1)
71 triggering the activation of IRF3 (IFN regulatory factor 3). This activation cascade leads to
72 the generation of type I interferons and inflammatory cytokines¹⁴. cGAS-STING is involved
73 in DNA repair, DNA damage responses (DDR) and cell senescence (reviewed in¹⁷). These
74 effects are achieved through the expression of interferon-stimulated genes (ISGs) and the
75 senescence-associated secretory phenotype (SASP)^{12,16}. Secretion of these molecules
76 modulates the proliferative capacity of surrounding cells in a paracrine manner,
77 propagating the senescence status (paracrine-SASP)¹⁸.

78 Type I interferon response is increasingly linked to aging and neurodegenerative
79 diseases across different species. A recent significant study by the Ablasser lab using
80 naturally aged mice revealed that cGAS–STING signaling plays a pivotal role in the age-
81 related type I interferon response in neurodegeneration¹⁹. Transcriptional profiling
82 revealed that cGAS–STING activation initiated a gene expression program shared
83 between neurodegenerative diseases and natural aging. The authors also observed that
84 there was an accumulation of mitochondrial DNA in the cell cytoplasm of microglial cells,
85 providing a potential mechanism through which the cGAS-STING pathway may contribute
86 to inflammation in the aging brain¹⁹.

87 *In vitro* studies using human primary cells recently showed that cGAS-STING is
88 activated by short or dysfunctional telomeres (reviewed in¹³). However, it is currently
89 unknown what are the consequences of activation of cGAS-STING in response to short
90 telomeres at the organism level. Here, we show that telomere shortening triggers cGAS-
91 STING pathway in skin, testis, kidney marrow (the adult hematopoietic organ in fish) and
92 intestine of zebrafish. This results in type I interferon response, elevation in senescence
93 levels and reduction in proliferative capacity of these tissues. Absence of cGAS-STING
94 restores cell proliferation, suppresses accelerated aging and increases in both health and
95 lifespan of the telomerase deficient zebrafish.

96

97 **Results (14998 characters/ 2212 words)**

98

99 **Telomere shortening activates the cGAS STING and type I interferon *in vivo***

100 Our previous studies show that telomerase deficient zebrafish undergo accelerated
101 systemic inflammation^{5-8,20,21}. Analysis of gene expression of proliferative (gut) and non-
102 proliferative tissues (muscle) derived from aged *tert*^{-/-} (9-months old) and WT (36-months
103 old) zebrafish highlighted several genes related to type I interferon response²⁰. To
104 investigate if short telomeres trigger type I inflammation and accelerated aging through the
105 cGAS-STING pathway, we combined *sting* zebrafish loss of function mutants
106 (*sting*^{sa35634/sa35634}, hereby referred to as *sting*^{-/-}) with telomerase deficient zebrafish
107 (*tert*^{hu3430/hu3430} or *tert*^{-/-}) extensively characterized in our previous studies^{5-8,21}. Upon
108 incross of double heterozygous fish, we first investigated if *tert*^{-/-} *sting*^{-/-} double mutants
109 had short telomeres comparable to their *tert*^{-/-} siblings. We observed that, by 9 months of
110 age, *tert*^{-/-} *sting*^{-/-} had similar mean telomere length to *tert*^{-/-} single mutants in the skin
111 and intestine (Figure 1A-D, Supplementary figure 1A-D). In testis, *tert*^{-/-} *sting*^{-/-} zebrafish
112 had slightly shorter telomeres than *tert*^{-/-} (Figure 1B, Supplementary Figure 1B) and
113 slightly longer telomeres in the kidney marrow (Figure 1C, Supplementary Figure 1C).
114 Overall, not only telomere length was similar between *tert*^{-/-} and *tert*^{-/-} *sting*^{-/-} but were
115 significantly shorter than WT and *sting*^{-/-} siblings.

116 Previous studies using cell lines reported that short and dysfunctional telomeres
117 lead to the formation of MN¹⁰⁻¹². To test whether we would observe an increase of MN
118 upon telomere shortening in zebrafish, we derived fibroblasts from the skin of 9-months old
119 animals. We observed a ten-fold increase in MN formation in *tert*^{-/-} zebrafish when
120 compared to the WT and *sting*^{-/-} siblings. Strikingly, *tert*^{-/-} *sting*^{-/-} had similar levels of MN
121 as *tert*^{-/-} siblings (Figure 1E). Thus, telomere shortening results in MN accumulation *in*
122 *vivo*.

123 After confirming the presence of shorter telomeres and MN in *tert*^{-/-} and *tert*^{-/-} *sting*^{-/-}
124 *sting*^{-/-} zebrafish, we investigated if the cGAS-STING pathway was active *in vivo* by quantifying
125 its downstream targets. Therefore, using skin of 9-months-old zebrafish, we analyzed the
126 phosphorylation status of zebrafish Tbk1 and Irf3 and the transcription level of two
127 members of type I interferon response, *isg15* and *ifn-i* (Figure 1F-H). Comparing *tert*^{-/-} to
128 WT zebrafish we observed ca. 3-fold increase in p-Irf3 and 2-fold increase in p-Tbk1
129 (Figure 1F). Consistently, expression of *isg15* and *ifn-i* was increased by 10- and 2.5-fold,
130 respectively (Figure 1G-H). However, the phosphorylation profile of Tbk1 and Irf3 in *tert*^{-/-}
131 *sting*^{-/-} mutants was similar to their WT and *sting*^{-/-} siblings (Figure 1F). *tert*^{-/-} *sting*^{-/-}

132 mutants also lacked type I interferon response, as observed by the reduced levels of *isg15*
133 and *ifn-i* (Figure 1G-H).

134 We expanded our study to other proliferative tissues like testis, kidney marrow and
135 intestine since they all show signs of inflammation in aging zebrafish^{5,8,21}. Comparing
136 transcription levels of *tert*^{-/-} fish to WT fish, we observed 15-fold increase in expression for
137 *isg15* and *ifn-i* in testis; 20-fold increase in *isg15* and 5 fold increase in kidney marrow;
138 and, lastly, 7.5-fold increase in *isg15* transcript and 2.5-fold increase in *ifn-i* in the intestine.
139 Importantly, inactive cGAS-STING pathway rescued the *isg15* and *ifn-i* levels of *tert*^{-/-}
140 *sting*^{-/-} to those observed in WT zebrafish in all tissues analyzed (Figure 1G, H). These
141 results show that, despite the presence of shorter telomeres and MN, the cGAS-STING
142 pathway is inactive in *tert*^{-/-} *sting*^{-/-} mutants.

143 Type I interferon response can be initiated by mobilization of transposable elements
144 (TEs). During replicative senescence of human fibroblasts, L1 retrotransposable elements
145 become transcriptionally derepressed and activate a type-I interferon response²². TE
146 transcription leads to robust activation of RIG-I and MDA5 that recognize dsRNA and
147 ssRNA and initiate a signaling cascade, involving MAVS oligomerization, IRF3/IRF7
148 activation and the expression of type I interferon response. We looked for the deregulation
149 of TEs expression in zebrafish testis, kidney marrow and intestine (Supplementary Fig. 2A-
150 B). Multidimensional scaling (MDS) plots of TE expression were non-overlapping for WT
151 and *tert*^{-/-} mutant in all tissues analyzed (Supplementary Fig. 2A). Telomerase-deficient
152 fish showed a clear upregulation of TEs in testis and kidney marrow and, to a lesser
153 extent, in the gut.

154 We then investigated whether the expressions of the RNA sensors *rig-I*, *mda5* and
155 *mavs* were increased in telomerase-deficient animals. Similar to TE expression, *rig-I* and
156 *mda5* were overexpressed in *tert*^{-/-} kidney marrow and testis, respectively, compared to
157 WT animals, but not the intestine (Supplementary Fig. 2C-D). Recently, the Karlseder lab
158 showed that both DNA sensing (cGAS-STING) and RNA sensing (ZBP1-MAVS) innate
159 immunity pathways orchestrate telomere replicative crisis (M2)²³. Their model proposes
160 that short telomeres and MN trigger cGAS-STING, whereas ZBP1 senses the telomeric
161 lncRNA TERRA and activates MAVS. Since both pathways result in the activation of type I
162 interferon response, we tested if ZBP1-MAVS could also contribute to IFN expression. As
163 zebrafish lack a clear *zbp1* gene orthologue, we relied solely on expression of *mavs* for
164 this analysis. *mavs* mRNA was significantly increased in the testis, but not in kidney
165 marrow and intestine (Supplementary Figure 2E). Thus, we observed that telomere

166 shortening triggers multiple responses that include TE expression deregulation and RNA
167 sensor pathway activation which, in turn, reinforce the expression of type I interferon.

168

169 **cGAS-STING is required for increased p53 levels in presence of DNA damage**

170 We previously reported that telomere shortening leads to increased p53 levels as a
171 consequence of activation of DDR in zebrafish^{5,6,8,21}. To identify the cause for activation of
172 cGAS-STING in prematurely aged *tert*^{-/-} mutants, we analyzed DNA damage and
173 activation of DDR in 9-month-old animals. First, we quantified the number of
174 phosphorylated H2AX (γ -H2AX) stained cells by immunofluorescence in the tissues of
175 interest. As in our previous work⁸, γ -H2AX staining was dispersed through the
176 nucleoplasm and aggregated in foci (Figure 2A insets). *tert*^{-/-} zebrafish displayed 3-fold
177 increase of γ -H2AX stained cells in the skin (Figure 2B), 4-fold in the testis (Figure 2C) and
178 5-fold increase both in the kidney marrow (Figure 2D) and the intestine (Figure 2E) when
179 compared to WT and *sting*^{-/-} mutants. Contrarily, *tert*^{-/-} *sting*^{-/-} mutants showed similar
180 levels of γ -H2AX compared to the *tert*^{-/-} sibling. (Figure 2A-D). Thus, consistent with
181 shorter telomere length in *tert*^{-/-} and *tert*^{-/-} *sting*^{-/-} mutants, we observed similar levels of
182 the DNA damage marker γ -H2AX in these tissues.

183 Increased γ -H2AX levels in *tert*^{-/-} zebrafish is accompanied by elevation in p53
184 protein levels^{8,21}. *tert*^{-/-} zebrafish exhibited an increase of 5-fold (Figure 2F,G) in the skin
185 and testis (Figure 2F,H), 3-fold in the kidney marrow (Figure 2F,I) and 6-fold in the
186 intestine (Figure 2F,J) when compared to WT and *sting*^{-/-} mutants (Figure 2E-H).
187 Surprisingly, p53 levels in the *tert*^{-/-} *sting*^{-/-} mutants were similar to the WT and *sting*^{-/-}
188 siblings (Figure 2F-J). Our results indicate that, despite similar levels of phosphorylated
189 H2AX, cGAS-STING is required for elevated p53 levels in response to telomere
190 shortening. This is in agreement with studies showing that p53 expression and stability are
191 regulated by IFNs^{24,25}.

192

193 **cGAS-STING is required for senescence and SASP caused by telomere shortening**

194 Given that p53 was not elevated in aging *tert*^{-/-} *sting*^{-/-} zebrafish, despite the
195 shorter telomere length, we decided to assess the remaining phenotypes linked with *tert*^{-/-}
196 premature aging. Previous studies in human cells showed that cGAS-STING is required
197 for cell senescence¹⁰⁻¹². Using 9-months-old zebrafish, we studied cell senescence using
198 the SA-Beta-Galactosidase (SA-B-gal) assay in addition to expression of *cdkn2a/b*
199 (p15/16) and *cdkn1a* (p21) by RT-qPCR. As previously observed^{5,6,8,21}, proliferative
200 tissues of *tert*^{-/-} mutants were strongly stained with SA-B-gal, but not those of WT or *sting*^{-/-}

201 *-/-* siblings (Figure 3A). Consistently, we confirmed an elevated expression of *cdkn2a/b* and
202 *cdkn1a* senescence markers in *tert-/-* mutants (Figure 3B-D). Senescence in *tert-/-* was
203 accompanied by expression of SASP-related genes, namely *il1b*, *tgfb1b* and *mmp15a*. As
204 expected, none of these genes were elevated in WT or *sting-/-* siblings (Figure 3B-D).

205 With lower levels of p53, cell senescence was also reduced in *tert-/- sting-/-* tissues,
206 as observed by low SA-Beta-gal and expression of *cdkn2a/b* and *cdkn1a*. In absence of
207 senescence, expression of SASP factors were also reduced in *tert-/- sting-/-* mutants to
208 the ones observed in WT (Figure 3B-D). Thus, in agreement with previous *in vitro* studies,
209 our results indicate that cGAS-STING is required for senescence and SASP of proliferative
210 tissues *in vivo*.

211

212 **cGAS-STING controls cell proliferation and tissue integrity of *tert-/-* zebrafish**

213 Replicative cell senescence is a barrier against cell proliferation in response to
214 telomere shortening. We thus investigated if absence of senescence in *tert-/- sting-/-*
215 mutants would result in increased cell proliferation. We examined proliferative tissues by
216 immunofluorescence using antibodies against PCNA, a marker for cell proliferation. As
217 previously reported^{5,6,8}, cell proliferation of *tert-/-* zebrafish is significantly reduced in
218 proliferative tissues when compared to WT and *sting-/-* siblings (Figure 4B-D). However,
219 lower cell proliferation was recovered to WT levels in *tert-/- sting-/-* zebrafish (Figure 4B-
220 D). Thus, with lower cell senescence and p53 levels, absence of cGAS-STING results in
221 an increase in cell proliferation despite telomere shortening in telomerase-deficient
222 zebrafish.

223 Previously, we showed that telomere shortening impacts tissue integrity and results
224 in morphological defects of several tissues^{5,6,8,21}. Inflammation of the intestine causes an
225 increase in thickness of the *lamina propria* in *tert-/-* zebrafish (mean of 17.5 micrometer,
226 Figure 4F-G). However, width of the *lamina propria* in *tert-/- sting-/-* zebrafish was similar
227 to the WT and *sting-/-* siblings (Figure 4G). Loss of gut tissue integrity activates the YAP-
228 TAZ pathway in aging *tert-/-* zebrafish⁸. In agreement, we observed an increase of *ctgf* and
229 *cyr61* levels, targets of YAP-TAZ pathway, (Figure 4L), in *tert-/-* zebrafish compared to WT
230 and *sting-/-* siblings. However, expressions of YAP-TAZ target genes were reduced to the
231 WT levels in the *tert-/- sting-/-* zebrafish (Figure 4L). Similarly, the remaining proliferative
232 tissues also showed increased expression of *ctgf* and *cyr61* in *tert-/-* zebrafish that were
233 absent in *tert-/- sting-/-* siblings (skin: 2.5-fold and 5-fold, respectively, kidney marrow: ~10
234 fold, Figure 4M, Supplementary Figure 4B-D). Thus, our results suggest that tissue

235 integrity of the intestine and other tissues caused by telomere shortening is rescued by an
236 increase of cell proliferation upon inactivation of the cGAS-STING pathway.

237

238 **cGAS-STING causes premature aging of *tert*^{-/-} zebrafish**

239 Given the previous results at the cellular level, we investigated the consequences to
240 the whole organism of absence cGAS-STING and Type I interferon in response to
241 telomere shortening. We previously established male fertility and testicular atrophy as
242 robust assays for aging zebrafish^{5,6,26}. To measure testicular atrophy, we quantified the
243 mature sperm area in HE stained sections of whole testis (Figure 4H). Percentage of
244 mature sperm area of 9-month-old *tert*^{-/-} zebrafish was reduced to ~5%, compared to
245 ~50% in WT and *sting*^{-/-} siblings (Figure 4I). However, the percentage of mature sperm
246 area increased to ~40% in *tert*^{-/-} *sting*^{-/-} zebrafish (Figure 4I). Denoting the observed loss
247 of tissue integrity in testis in *tert*^{-/-} prematurely aged zebrafish, we saw increased
248 expression of the YAP-TAZ pathway targets in *ctgf* and *cyr61* compared to WT and *sting*^{-/-}
249 siblings (Figure 4M). Consistent with our previous results, expression of *ctgf* and *cyr61*
250 were reduced in *tert*^{-/-} *sting*^{-/-} to WT levels (Figure 4M).

251 We next asked if the rescue in the testis morphology of *tert*^{-/-} *sting*^{-/-} would restore
252 fertility of aging *tert*^{-/-} zebrafish. We previously reported that, from 6-month-old, *tert*^{-/-}
253 males become infertile paralleling the loss fertility observed in 18-month-old WT fish⁵. As
254 expected, 9-month-old *tert*^{-/-} males were unable to produce fertilized eggs when crossed
255 with young WT females (Figure 5A). Strikingly, *tert*^{-/-} *sting*^{-/-} males were still fertile even if
256 slightly lower than the WT and *sting*^{-/-} siblings (Figure 5A). Our data shows that inhibition
257 of cGAS-STING and type I interferon response is sufficient to restore fertility to aging *tert*^{-/-}
258 zebrafish.

259 As other vertebrates, incidence of cancer increases with age in zebrafish^{5,26,27}.
260 Similar to other age-associated phenotypes, the spontaneous cancer incidence is
261 accelerated in younger ages in *tert*^{-/-} zebrafish^{5,26}. We quantified the rate of spontaneous
262 tumor formation, mostly seminomas, in male zebrafish. We observed that *tert*^{-/-} zebrafish
263 developed tumors from the age of 11-month-old and by the age of 17 months (Figure 5D).
264 Strikingly, *tert*^{-/-} *sting*^{-/-} mutants developed macroscopic tumors around the age of 12
265 months but were restricted to 5% of the population (Figure 5D). Importantly, spontaneous
266 cancer incidence of *tert*^{-/-} *sting*^{-/-} zebrafish was not statistically different from the WT and
267 *sting*^{-/-} siblings.

268 Other phenotypes of aging, such as kyphosis (abnormal curvature of the spine),
269 caused by increased weakness of the spinal bones, and cachexia (excessive muscle

270 wasting), caused by muscle tissue atrophy, are present in younger *tert*^{-/-} mutants and only
271 appear later in WT zebrafish^{5,6}. By the age of 15 months, 60% of *tert*^{-/-} zebrafish showed
272 aging phenotypes (Figure 5B) and weighed significantly less (Figure 5C) than WT and
273 *sting*^{-/-} siblings. However, the incidence of aging phenotypes ameliorated in *tert*^{-/-} *sting*^{-/-}
274 mutants (Figure 5B) and weight was restored to WT levels (Figure 5C).

275 Finally, we compared the lifespan of *tert*^{-/-} mutants to their *tert*^{-/-} *sting*^{-/-} siblings.
276 Whereas *tert*^{-/-} mutants had a mean lifespan of 17 months-old, lifespan was extended to
277 24 months in *tert*^{-/-} *sting*^{-/-} mutants (Figure 5E). The mean lifespan of *tert*^{-/-} *sting*^{-/-}
278 zebrafish was not statistically different from WT and *sting*^{-/-} siblings (Figure 5F). Overall,
279 our results show that by inhibiting cGAS-STING and, consequently, type I interferon, we
280 observed an increase in lifespan of a prematurely aging vertebrate model by 41%. More
281 importantly, we recover most age-associated phenotypes of aging *tert*^{-/-} mutants,
282 increasing their healthspan without the increase in cancer incidence.

283

284 **Discussion (7452 characters/1053 words)**

285 Aging is accompanied by a wide range of physiological changes, such as chronic
286 inflammation²⁸. Age-associated inflammation in absence of overt infection has been
287 termed inflammaging²⁹. While the origins of inflammaging are mostly unclear, it is typically
288 characterized by high levels of pro-inflammatory cytokines, chemokines, acute phase
289 proteins, and soluble cytokine receptors in the serum^{29,30}. Inflammaging was shown to
290 contribute to the development of age-associated diseases, such as neurodegenerative
291 diseases, cardiovascular diseases and cancer²⁸. These are the main causes of morbidity
292 and mortality in the elderly. Recent exciting new data revealed that DNA damage and
293 inflammation are connected by the cGAS-STING pathway^{10,12,31}. Moreover, chemical
294 inhibition of STING suppresses aging-associated inflammation and neurodegeneration¹⁹.
295 Our study extends these observations by showing that activation of cGAS-STING pathway
296 caused by telomere shortening is responsible for premature aging in zebrafish.

297 What triggers inflammaging upon telomere shortening? We documented several
298 potential triggers for type I interferon responses in our work. We observed an increase of
299 MN in *tert*^{-/-} zebrafish. However, recent data has shown that, even though cGAS is
300 recruited to MN, the presence of chromatin might not lead to elevated cGAMP and STING
301 activation³². Further evidence from aging mice showed that mtDNA released from
302 disrupted mitochondria was an important source for cGAS-STING activation¹⁹. In our
303 previous work²¹, we showed that telomerase mutants have dysfunctional mitochondria with
304 disrupted membranes providing a likely source for cytoplasmic mtDNA as an additional

305 trigger. Moreover, mirroring what was previously observed in human fibroblasts^{22,23}, we
306 documented a tissue-specific elevation of TE expression, accompanied by increased
307 expression of the RNA sensing pathway Rig-I, Mda5 and Mavs, that contribute and likely
308 reinforce the activation type I interferon during aging. Finally, expression of the telomeric
309 lncRNA TERRA could also contribute to the activation of cGAS-STING via the
310 ZBP1/MAVS pathway, as reported for p53-deficient human cells undergoing crisis²³.
311 However, we were unable to detect a clear elevation of *mavs* expression in all tissues. A
312 likely explanation may relate to *tert*^{-/-} zebrafish being p53 proficient and, therefore, their
313 comparatively longer telomeres may not express sufficient levels of TERRA to trigger its
314 response.

315 Our work reveals that DDR and senescence triggered by short telomeres require an
316 active cGAS-STING pathway. Even though telomere length and γ -H2AX levels were
317 similar between *tert*^{-/-} and *tert*^{-/-} *sting*^{-/-} zebrafish, p53 was only elevated in *tert*^{-/-}
318 mutants. Although a definite explanation is currently unavailable, we suggest potential
319 leads for this observation. First, IFN- β signaling was shown to induce p53 transcription²⁵.
320 Therefore, cGAS-STING may be required to promote p53 expression independently of
321 canonical DDR. Second, the interferon-stimulated gene ISG15, an ubiquitin-like protein, is
322 involved in p53 degradation by the 20S proteasome. ISG15 primarily targets misfolded
323 p53 and deletion of ISG15 results in suppression of p53 activity and functions²⁴. Thus,
324 absence of cGAS-STING may lead to p53 destabilization. Third, cGAS-STING may
325 sensitize cells to DNA damage by lowering the threshold for DDR activation. In absence of
326 cGAS-STING, the ATM/ATR-p53 pathway may remain ineffective until genome instability
327 is triggered by telomere-end fusions during crisis. In this scenario, phosphorylation of γ -
328 H2AX could be achieved through parallel pathways, such as DNA-PKcs.

329 Absence of cGAS-STING in aging telomerase deficient zebrafish results in low p53
330 levels, reduced senescence and increased cell proliferation, thus rescuing damage
331 imposed to proliferative tissues. This phenotype is also observed in *tp53*^{-/-} *tert*^{-/-} double
332 mutant zebrafish²⁶. Similar to late-generation telomerase deficient mice³³, lack of p53
333 leads to organismal rescue and increased fertility allowing for extra generations with ever-
334 shorter telomere mice³⁴. As first observed in tissue culture, upon telomere shortening, the
335 first barrier to cell proliferation (M1) is imposed by p53/Rb and occurs when telomeres are
336 long enough to allow for further cell divisions³⁵. With loss of p53, the ensuing cell
337 proliferation results in complete telomere deprotection, genome instability and cell death
338 during crisis (M2)³¹. In this context, loss of cGAS-STING response is consistent with loss
339 of p53 in aging *tert*^{-/-} mutants. However, *tert*^{-/-} *sting*^{-/-} do not completely phenocopy *tert*^{-/-}

340 *tp53*^{-/-} mutants. Loss of cGAS-STING does not cause an increase in spontaneous tumor
341 incidence of either WT or *tert*^{-/-} zebrafish. Zebrafish lacking p53, die prematurely primarily
342 from increased soft tissue tumors³⁶. In contrast, *tert*^{-/-} *sting*^{-/-} zebrafish lack elevated
343 tumorigenesis characteristic of *tert*^{-/-} *tp53*^{-/-} mutants²⁶. This may be attributed to the
344 downstream consequences of cGAS-STING and type I interferon response. Chronic
345 inflammation may be a key component of increased tumorigenesis in *tp53*^{-/-} mutants. Lack
346 of inflammatory responses may protect *tert*^{-/-} *sting*^{-/-} zebrafish from early tumorigenesis in
347 face of increasing DNA damage.

348 We found that inhibiting cGAS-STING would restore tissue integrity and reduce
349 expression of YAP-TAZ target genes in aging *tert*^{-/-} mutants⁸. The YAP-TAZ pathway was
350 recently shown to regulate cGAS-STING in stromal and contractile cells of aging mice³⁷.
351 Mechanotransduction by YAP-TAZ suppresses the activity of cGAS-STING, preventing
352 senescence *in vivo* and tissue degeneration of prematurely aging mouse models³⁷. Our
353 work now shows that cGAS-STING is also required for YAP-TAZ activity upon telomere
354 shortening. This is likely to be the result of an indirect effect on tissue architecture.
355 Restoring tissue integrity would reduce the activation of YAP-TAZ mechanosignaling and
356 modifications to the extracellular matrix.

357 Loss of cGAS-STING and type I interferon improved the healthspan and the
358 lifespan of aging *tert*^{-/-} mutants. Telomere shortening does not occur simultaneously in all
359 tissues in humans and zebrafish^{5,38}. The gut of aging zebrafish presents early dysfunction
360 and telomere shortening. We have recently shown that expressing telomerase specifically
361 in the gut of *tert*^{-/-} mutants prevents telomere shortening and gut dysfunction⁸. More
362 importantly, maintaining telomere length in the gut also reverses remote organ dysfunction
363 and longevity of the entire organism. Like *tert*^{-/-} *sting*^{-/-} zebrafish, gut-specific telomerase
364 expression in *tert*^{-/-} mutants reduces p53 levels and cell senescence in proliferative
365 organs, namely testis and kidney marrow, despite short telomeres and increased levels of
366 γ -H2AX. These lead to increased cell proliferation and restored tissue integrity. We
367 propose that cGAS-STING and type I interferon responses initiated by telomere shortening
368 in specific organs of aging individuals result in systemic chronic inflammation
369 (inflammaging) deteriorating tissue integrity of remote organs by increasing DNA damage
370 and reducing cell proliferation. Thus, inhibition of STING and chronic inflammation in
371 organs primarily affected by telomere shortening, such as the gut and blood, would
372 increase healthspan and lifespan. This provides a new approach for treatments of
373 telomere biology disorders and to improve healthy aging.

374

375 **Materials and Methods:**

376

377 **Ethics statement**

378 The zebrafish work was conducted according to local and international institutional
379 guidelines and was approved in Portugal by the Ethics Committee of the Instituto
380 Gulbenkian de Ciência and approved by the competent Portuguese authority (Direcção
381 Geral de Alimentação e Veterinária; approval no. 0421/000/000/2015) and in France by
382 the Animal Care Committee of the Institute for Research on Cancer and Aging, Nice, the
383 regional (CIEPAL Côte d'Azur no. 697) and national (French Ministry of Research no.
384 27673-2020092817202619) authorities.

385

386 **Zebrafish lines and maintenance**

387 Zebrafish were maintained in accordance with Institutional and National animal care
388 protocols. To ensure telomere length comparisons and avoid the effects of
389 haploinsufficiency of *tert*^{+/-} heterozygous parental fish, we maintained double
390 heterozygous stock lines (*tert*^{AB/hu340} *sting*^{AB/sa35631}) as outcrosses to WT AB zebrafish.
391 Experimental fish were obtained incrossing the stock fish. The overall characterization of
392 these four genotypes was performed in F1 sibling animals at 9 months of age. Due to male
393 sex bias in our crosses, that affected mostly *tert*^{-/-} progeny, we were unable to obtain
394 significant numbers of females for analysis and so all of our data except survival analysis
395 are restricted to males.

396

397 **Telomere restriction fragment (TRF) analysis by Southern blot**

398 Isolated tissues were first lysed at 50°C overnight in lysis buffer (Fermentas #K0512)
399 supplemented with 1mg/ml Proteinase K (Sigma Aldrich) and RNase A (1:100 dilution,
400 Sigma Aldrich). Genomic DNA was then extracted by equilibrated phenol-chloroform
401 (Sigma Aldrich) and chloroform-isoamyl alcohol extraction (Sigma Aldrich). The same
402 amount of gDNA was digested with *RS*I and *H*INFI enzymes (NEB) for 12 h at 37°C.
403 After digestion, samples were loaded on a 0.6% agarose gel, in 0.5% TBE buffer, and run
404 on an electrophoresis apparatus (Bio-Rad). The electrophoresis conditions were 110 V for
405 15 h. Gels were then processed for Southern blotting using a 1.6 kb telomere probe,
406 (TTAGGG)_n, labeled with [alpha-32P]-dCTP.

407

408 **Fibroblast Derival**

409 9-month-old fish zebrafish were sacrificed in 1g/L of MS-222 (Sigma Aldrich), and the skin
410 was collected in PBS. After 3 washes in PBS + 2% antibiotics (Penicillin/Streptomycin,
411 Gentamycin and Amphotericin b), the skin was dissociated for 5 minutes in Tryple (Gibco),
412 cut into small pieces, and let to adhere O/N on coverslip coated by gelatin 2% in presence
413 of few drops of FBS + 2% antibiotics. The day after, when the first fibroblasts were
414 released from the skin, the well was filled with DMEM + 2% antibiotics. After 48h,
415 fibroblasts were fixed and DAPI staining was performed.

416

417 **Western Blot**

418 Age and sex matched adult zebrafish were sacrificed in 1g/L of MS-222 (Sigma Aldrich)
419 and collected tissues (skin, testis, kidney marrow and intestine) were immediately snap
420 frozen liquid nitrogen. Tissues were homogenized in RIPA buffer (sodium chloride 150
421 mM; Triton-X-100 1%, sodium deoxycholate 0.5%, SDS 0.1%, Tris 50 mM, pH=8.0),
422 including complete protease and phosphatase inhibitor cocktails (Roche diagnostics) with
423 a motor pestle on ice. Homogenized tissues were incubated for 30 minutes on ice and
424 centrifuged at 4°C, 13.000 rpm for 10 min. Supernatant was collected and stored at -80°C
425 until use.

426 For each sample, 50 µg of protein was loaded per well, separated on 10% SDS-PAGE
 427 gels and transferred to Nitrocellulose Membrane (BioRad #1620097). The membranes
 428 were blocked in 5% milk and then incubated with the primary antibody overnight at 4°C.
 429 Antibody complexes were visualized by enhanced chemiluminescence (ECL) after
 430 incubation with the appropriate HRP-conjugated secondary antibody. Antibodies
 431 concentrations: anti-p53 (1:1000, Anaspec, 55342), anti TBK1 (1:1000, CST, 3504), anti
 432 pTBK1 (1:1000, CST, 5483), anti IRF3 (1:1000, CST, 11904), anti pIRF3 (1:1000, CST,
 433 29047).

434

435 Real-time quantitative PCR

436 Age and sex matched adult zebrafish were sacrificed in 1g/L of MS-222 (Sigma Aldrich)
 437 and collected tissues (skin, testis, kidney marrow and intestine) were immediately snap
 438 frozen liquid nitrogen. RNA extractions were performed in TRIzol (Invitrogen) by mashing
 439 tissues with a motorized pestle in a 1.5 mL eppendorf tube. After incubation at room
 440 temperature (RT) for 10 min TRIzol, chloroform extractions were performed. Quality of
 441 RNA samples was assessed through BioAnalyzer (Agilent 2100). Retro-transcription into
 442 cDNA was performed using QuantiTect Reverse Transcription kit (Qiagen).

443 Quantitative PCR (qPCR) was performed using FastStart Universal SYBR Green Master
 444 mix (Roche) and an StepOne+ Real time PCR Detection System (Applied Biosystems).
 445 qPCRs were carried out in duplicate for each cDNA sample. Relative mRNA expression
 446 was normalized against *rps11* mRNA expression using the $2^{-\Delta\Delta CT}$ method.

447

	Gene ID:	Forward primer	Reverse primer
<i>isg15</i>	ZDB-GENE-021211-1	ACTCGGTGACGATGCAGC	TGGGCACGTTGAAGTACTGA
<i>ifn-i</i>	ZDB-GENE-030721-3	CAAGATACGCAAAGCCAGCA	GTGGCTTTTCACAACCTCTCC
<i>cdkn2a/b</i>	ZDB-GENE-081104-306	GAGGATGAACTGACCACAGCA	CAAGAGCCAAAGGTGCGTTAC
<i>cdkn1a</i>	ZDB-GENE-070705-7	CAGCGGGTTTACAGTTTCAGC	TGAACGTAGGATCCGCTTGT
<i>il1b</i>	ZDB-GENE-040702-2	CGCTCCACATCTCGTACTCA	ATACGCGGTGCTGATAAACC
<i>tgfb1b</i>	ZDB-GENE-091028-1	ACCCCAGTTCAGCACACCATAG	TCGAAACTCGGCCTGGTAGA
<i>mmp15a</i>	ZDB-GENE-070817-4	GGGTCATGCTCTGGGGTTGG	AGTGGTGACAGTCTCTGGAGATCC A
<i>ctgf</i>	ZDB-GENE-030131-102	ACTCCCCTCGTCAAACACC	GGGACCGTATGTCTCCTCCT
<i>cyr61</i>	ZDB-GENE-040426-3	CCGTGTCCACATGTACATGGG	GGTGCATGAAAGAAGCTCGTC
<i>mavs</i>	ZDB-GENE-070112-1402	AGTAGAAGCCGCGAGAGGTA	GGCTTCGATCTCTCCCGAT
<i>rps11</i>	ZDB-GENE-040426-2701	ACAGAAATGCCCTTCACTG	GCCTCTTCTCAAACGGTTG

448

449 Histology

450 Age and sex-matched adult zebrafish were sacrificed in 1g/L of MS-222 (Sigma Aldrich),
 451 fixed for 72 hours in 4% paraformaldehyde and decalcified in 0.5M EDTA for 48 hours at
 452 room temperature. Whole fish were then paraffin-embedded to perform five micrometer
 453 sagittal section slides. Slides were stained with hematoxylin (Sigma Aldrich) and eosin
 454 (Sigma Aldrich) for histopathological analysis. Microphotographs (N>=6 fish per genotype)
 455 were acquired in a Leica DM4000 B microscope coupled to a Leica DFC425 C camera
 456 (Leica Microsystems).

457

458

Immunofluorescence

459

460

461

462

463

464

465

466

467

468

469

470

471

472

473

474

475

476

477

Senescence Associated Beta Galactosidase Staining

478

479

480

481

482

483

484

485

486

487

Fertility assays

488

489

490

491

492

493

494

495

496

497

Fixation for histology and tumor evaluation

498

499

500

501

502

503

504

RNA-seq analysis of TE families.

505

506

507

508

Raw FASTQ read files obtained from the SRA (PRJNA937311) were aligned to the reference zebrafish genome (GRCz10/danRer10) using STAR v2.7.10a with the following parameters to retain multi-mapping reads: --outMultimapperOrder Random --outSAMmultNmax 1 --outFilterMismatchNmax 3 --winAnchorMultimapperNmax 100 --

509 outFilterMultimapNmax 100 --alignSJDBoverhangMin 1. Expression of transposable
510 element families was quantified using Tetrascripts v2.2.393 with parameter `--mode=multi`
511 to estimate transposable element abundances from multimapped alignments using the
512 pre-generated GENCODE danRer10 TE GTF file from the Hammel lab FTP site
513 (https://labshare.cshl.edu/shares/mhammellab/www-data/Tetrascripts/TE_GTF). Counts
514 were normalized to counts per million (CPM) and differential expression was assessed in
515 R v3.1.4 (R Core Team, 2022) on the combined transposable element /gene counts using
516 the edgeR package v3.34.189 exact test.

517

518 **Statistical Analysis**

519 Graphs and statistical analyses were performed in GraphPad Prism8 software, using one-
520 way ANOVA test Tukey's post-correction or unpaired t-test. A critical value for significance
521 of $p < 0.05$ was used throughout the study. For survival analysis, Log-rank tests were
522 performed using GraphPad Prism8 to determine statistical differences of survival curves.

523

524

525 **Data availability**

526 All data generated or analyzed during this study are included in this published article and
527 its Extended information files.

528

529

530 **Acknowledgments**

531 We are grateful to our team members for fruitful discussions and advice. Especially, we
532 thank Dr. Hervé Técher for critically reading the manuscript. This work was supported by
533 the Université Côte d'Azur - Académie 4 (Installation Grant: Action 2 - 2019) and Institut
534 National du Cancer (INCa, PLBIO21-228). N.S. was supported by a PhD fellowship by La
535 Ligue Contre le Cancer. E.T. and P.B. thank the German Research Foundation, grant nos.
536 322977937/GRK2344. We are grateful to the PEMAV fish facility, Imaging core facility
537 (PICMI) and the Genomics facilities at the IRCAN supported by FEDER, Région Provence
538 Alpes-Côte d'Azur, Conseil Départemental 06, ITMO Cancer Aviesan (plan cancer),
539 Cancéropole Provence Alpes-Côte d'Azur, Gis Ibisa, CNRS and Inserm. The funders had
540 no role in study design, data collection and analysis, decision to publish or preparation of
541 the manuscript.

542

543 **Author contributions**

544 N.S. performed most experiments and carried out data analyses. G.A. performed data
545 analysis and revised the manuscript. B.L.-B. performed the skin fibroblast cell derivation
546 and micronuclei quantifications. M.M. proposed the idea for the study and performed the
547 initial analysis of the *sting*^{-/-} *tert*^{-/-} double mutants. RNA-seq analysis of transposon
548 elements was performed by P.B. and supervised by E.T. N.S. and M.G.F. designed the
549 experiments and wrote the manuscript. M.G.F. conceived the study, acquired funding and
550 supervised the work.

551

552 **Declaration of competing interests**

553 The authors declare no competing interests.

554

555 References

- 556 1. Armanios, M. Syndromes of telomere shortening. *Annu Rev Genomics Hum Genet* **10**, 45–61
557 (2009).
- 558 2. Mitchell, J. R., Wood, E. & Collins, K. A telomerase component is defective in the human
559 disease dyskeratosis congenita. *Nature* **402**, 551–5 (1999).
- 560 3. Opresko, P. L. & Shay, J. W. Telomere-associated aging disorders. *Ageing Res Rev* **33**, 52–
561 66 (2017).
- 562 4. Anchelin, M. *et al.* Premature aging in telomerase-deficient zebrafish. *Dis Model Mech*
563 (2013) doi:10.1242/dmm.011635.
- 564 5. Carneiro, M. C. *et al.* Short Telomeres in Key Tissues Initiate Local and Systemic Aging in
565 Zebrafish. *PLoS Genet* **12**, e1005798 (2016).
- 566 6. Henriques, C. M., Carneiro, M. C., Tenente, I. M., Jacinto, A. & Ferreira, M. G. Telomerase
567 is required for zebrafish lifespan. *PLoS Genet* **9**, e1003214 (2013).
- 568 7. Lex, K. *et al.* Telomere shortening produces an inflammatory environment that increases
569 tumor incidence in zebrafish. *Proc Natl Acad Sci U S A* **117**, 15066–15074 (2020).
- 570 8. El Maï, M. *et al.* Gut-specific telomerase expression counteracts systemic aging in
571 telomerase-deficient zebrafish. *Nat Aging* **3**, 567–584 (2023).
- 572 9. Oh, H. S.-H. *et al.* Organ aging signatures in the plasma proteome track health and disease.
573 *Nature* **624**, 164–172 (2023).
- 574 10. Glück, S. *et al.* Innate immune sensing of cytosolic chromatin fragments through cGAS
575 promotes senescence. *Nat Cell Biol* **19**, 1061–1070 (2017).
- 576 11. Yang, H., Wang, H., Ren, J., Chen, Q. & Chen, Z. J. cGAS is essential for cellular
577 senescence. *Proc Natl Acad Sci U S A* **114**, E4612–E4620 (2017).
- 578 12. Dou, Z. *et al.* Cytoplasmic chromatin triggers inflammation in senescence and cancer. *Nature*
579 **550**, 402–406 (2017).
- 580 13. Nassour, J., Przetocka, S. & Karlseder, J. Telomeres as hotspots for innate immunity and
581 inflammation. *DNA Repair (Amst)* **133**, 103591 (2024).
- 582 14. Motwani, M., Pesiridis, S. & Fitzgerald, K. A. DNA sensing by the cGAS–STING pathway
583 in health and disease. *Nat Rev Genet* **20**, 657–674 (2019).
- 584 15. Sun, L., Wu, J., Du, F., Chen, X. & Chen, Z. J. Cyclic GMP-AMP synthase is a cytosolic
585 DNA sensor that activates the type I interferon pathway. *Science* **339**, 786–91 (2013).
- 586 16. Ishikawa, H. & Barber, G. N. STING is an endoplasmic reticulum adaptor that facilitates
587 innate immune signalling. *Nature* **455**, 674–8 (2008).
- 588 17. Zierhut, C. Potential cGAS-STING pathway functions in DNA damage responses, DNA
589 replication and DNA repair. *DNA Repair (Amst)* **133**, 103608 (2024).
- 590 18. Glück, S. & Ablasser, A. Innate immunosensing of DNA in cellular senescence. *Curr Opin*
591 *Immunol* **56**, 31–36 (2019).
- 592 19. Gulen, M. F. *et al.* cGAS-STING drives ageing-related inflammation and neurodegeneration.
593 *Nature* **620**, 374–380 (2023).
- 594 20. Carneiro Madalena. The role of short telomeres as cause of natural aging in zebrafish.
595 (Universidade Nova de Lisboa, Lisboa, Portugal, 2015).
- 596 21. El Maï, M., Marzullo, M., de Castro, I. P. & Ferreira, M. G. Opposing p53 and mTOR/AKT
597 promote an in vivo switch from apoptosis to senescence upon telomere shortening in
598 zebrafish. *Elife* **9**, (2020).
- 599 22. De Cecco, M. *et al.* L1 drives IFN in senescent cells and promotes age-associated
600 inflammation. *Nature* **566**, 73–78 (2019).
- 601 23. Nassour, J. *et al.* Telomere-to-mitochondria signalling by ZBP1 mediates replicative crisis.
602 *Nature* **614**, 767–773 (2023).
- 603 24. Huang, Y.-F., Wee, S., Gunaratne, J., Lane, D. P. & Bulavin, D. V. Isg15 controls p53
604 stability and functions. *Cell Cycle* **13**, 2200–10 (2014).
- 605 25. Takaoka, A. *et al.* Integration of interferon-alpha/beta signalling to p53 responses in tumour
606 suppression and antiviral defence. *Nature* **424**, 516–23 (2003).

- 607 26. Şerifoğlu, N., Lopes-Bastos, B. & Ferreira, M. G. Lack of telomerase reduces cancer
608 incidence and increases lifespan of zebrafish tp53M214K mutants. *Sci Rep* **14**, 5382 (2024).
- 609 27. Spitsbergen, J. M., Buhler, D. R. & Peterson, T. S. Neoplasia and neoplasm-associated
610 lesions in laboratory colonies of zebrafish emphasizing key influences of diet and
611 aquaculture system design. *ILAR J* **53**, 114–25 (2012).
- 612 28. López-Otín, C., Blasco, M. A., Partridge, L., Serrano, M. & Kroemer, G. Hallmarks of aging:
613 An expanding universe. *Cell* **186**, 243–278 (2023).
- 614 29. Franceschi, C., Garagnani, P., Parini, P., Giuliani, C. & Santoro, A. Inflammaging: a new
615 immune-metabolic viewpoint for age-related diseases. *Nat Rev Endocrinol* **14**, 576–590
616 (2018).
- 617 30. Li, X. *et al.* Inflammation and aging: signaling pathways and intervention therapies. *Signal*
618 *Transduct Target Ther* **8**, 239 (2023).
- 619 31. Nassour, J. *et al.* Autophagic cell death restricts chromosomal instability during replicative
620 crisis. *Nature* **565**, 659–663 (2019).
- 621 32. Sato, Y. & Hayashi, M. T. Micronucleus is not a potent inducer of the cGAS/STING
622 pathway. *Life Sci Alliance* **7**, (2024).
- 623 33. Rudolph, K. L. *et al.* Longevity, Stress Response, and Cancer in Aging Telomerase-Deficient
624 Mice. *Cell* **96**, 701–712 (1999).
- 625 34. Chin, L. *et al.* p53 deficiency rescues the adverse effects of telomere loss and cooperates
626 with telomere dysfunction to accelerate carcinogenesis. *Cell* **97**, 527–38 (1999).
- 627 35. Saretzki, G., Sitte, N., Merkel, U., Wurm, R. E. & von Zglinicki, T. Telomere shortening
628 triggers a p53-dependent cell cycle arrest via accumulation of G-rich single stranded DNA
629 fragments. *Oncogene* **18**, 5148–58 (1999).
- 630 36. Berghmans, S. *et al.* tp53 mutant zebrafish develop malignant peripheral nerve sheath
631 tumors. *Proc Natl Acad Sci U S A* **102**, 407–12 (2005).
- 632 37. Sladitschek-Martens, H. L. *et al.* YAP/TAZ activity in stromal cells prevents ageing by
633 controlling cGAS-STING. *Nature* **607**, 790–798 (2022).
- 634 38. Aubert, G., Baerlocher, G. M., Vulto, I., Poon, S. S. & Lansdorp, P. M. Collapse of telomere
635 homeostasis in hematopoietic cells caused by heterozygous mutations in telomerase genes.
636 *PLoS Genet* **8**, e1002696 (2012).
- 637
- 638

639 Figure Legends

640

641 **Figure 1: Telomere shortening activates cGAS-STING pathway.** **a**, quantification of mean
642 telomere length measured by TRF analysis in the skin ($n_{WT}=5$, $n_{tert-/-}=5$, $n_{sting-/-}=5$, $tert-/-\ sting-/-=4$, WT
643 vs $tert-/-$ $p=0.017$, $tert-/-$ vs $sting-/-$ $p=0.002$, $sting-/-$ vs $tert-/-\ sting-/-$ $p=0.008$). **b**, quantification of
644 mean telomere length measured by TRF analysis in the testis ($n_{WT}=4$, $n_{tert-/-}=6$, $n_{sting-/-}=5$, $tert-/-\ sting-/-$
645 $=6$, WT vs $tert-/-$ $p=0.001$, WT vs $tert-/-\ sting-/-$ $p<0.001$, $tert-/-$ vs $sting-/-$ $p=0.016$, $sting-/-$ vs $tert-/-$
646 $sting-/-$ $p=0.001$). **c**, quantification of mean telomere length measured by TRF analysis in the
647 kidney marrow ($n_{WT}=3$, $n_{tert-/-}=4$, $n_{sting-/-}=7$, $tert-/-\ sting-/-=7$, WT vs $tert-/-$ $p<0.001$, WT vs $tert-/-\ sting-/-$
648 $p=0.001$, $tert-/-$ vs $sting-/-$ $p<0.001$, $sting-/-$ vs $tert-/-\ sting-/-$ $p<0.001$, $tert-/-$ vs $tert-/-\ sting-/-$
649 $p=0.003$). **d**, quantification of mean telomere length measured by TRF analysis in the intestine
650 ($n_{WT}=6$, $n_{tert-/-}=6$, $n_{sting-/-}=6$, $tert-/-\ sting-/-=6$, WT vs $tert-/-$ $p=0.001$, WT vs $tert-/-\ sting-/-$ $p=0.015$, $tert-/-$
651 vs $sting-/-$ $p<0.001$, $sting-/-$ vs $tert-/-\ sting-/-$ $p=0.008$, $p=0.623$). **e**, representative
652 immunofluorescence images and quantifications of MN formation in the fibroblasts derived from
653 skin ($n_{WT}=1$, $n_{tert-/-}=1$, $n_{sting-/-}=1$, $tert-/-\ sting-/-=1$, WT vs $tert-/-$ $p=0.040$, WT vs $tert-/-\ sting-/-$ $p=0.034$,
654 $tert-/-$ vs $sting-/-$ $p=0.047$, $sting-/-$ vs $tert-/-\ sting-/-$ $p=0.040$). **f**, representative western blot images
655 and quantification of downstream targets of cGAS-STING pathway ($n_{WT}=4-5$, $n_{tert-/-}=5-6$, $n_{sting-/-}=5-7$,
656 $tert-/-\ sting-/-=5$, $p-Irf3/Irf3$: WT vs $tert-/-$ $p=0.049$, $tert-/-$ vs $tert-/-\ sting-/-$ $p=0.011$; $p-Tbk1/Tbk1$: WT
657 vs $tert-/-$ $p=0.035$, $tert-/-$ vs $sting-/-$ $p=0.002$, $tert-/-$ vs $tert-/-\ sting-/-$ $p=0.042$). **g**, RT-qPCR
658 analysis of *isg15* gene expression in the skin, testis, kidney marrow and intestine ($n_{WT}=5-6$, $n_{tert-/-}$
659 $=4-8$, $n_{sting-/-}=5-8$, $tert-/-\ sting-/-=7-9$, skin: WT vs $tert-/-$ $p=0.024$, $sting-/-$ vs $tert-/-$ $p=0.011$, $N=5-7$, $tert-/-$
660 vs $tert-/-\ sting-/-$ $p=0.007$; testis: WT vs $tert-/-$ $p=0.001$, $sting-/-$ vs $tert-/-$ $p=0.001$, $tert-/-$ vs $tert-/-$
661 $sting-/-$ $p=0.002$; kidney marrow: $N=6-9$, WT vs $tert-/-$ $p=0.045$, $sting-/-$ vs $tert-/-$ $p=0.022$, $tert-/-$ vs
662 $tert-/-\ sting-/-$ $p=0.019$; intestine: WT vs $tert-/-$ $p<0.001$, $sting-/-$ vs $tert-/-$ $p<0.001$, $tert-/-$ vs $tert-/-$
663 $sting-/-$ $p=0.001$). **h**, RT-qPCR analysis of *ifn-i* gene expression in the skin, testis, kidney marrow
664 and intestine ($n_{WT}=4-6$, $n_{tert-/-}=5-8$, $n_{sting-/-}=5-8$, $tert-/-\ sting-/-=6-9$, skin: $sting-/-$ vs $tert-/-$ $p=0.004$, $tert-/-$
665 vs $tert-/-\ sting-/-$ $p=0.002$; testis: WT vs $tert-/-$ $p=0.003$, $sting-/-$ vs $tert-/-$ $p=0.003$, $tert-/-$ vs $tert-/-$
666 $sting-/-$ $p=0.003$; kidney marrow: WT vs $tert-/-$ $p=0.008$, $sting-/-$ vs $tert-/-$ $p=0.004$, $tert-/-$ vs $tert-/-$
667 $sting-/-$ $p=0.011$; intestine: WT vs $tert-/-$ $p=0.020$, $sting-/-$ vs $tert-/-$ $p=0.005$, $tert-/-$ vs $tert-/-\ sting-/-$
668 $p=0.014$). Data are presented as the mean \pm s.e.m.; * $p<0.05$; ** $p<0.01$, *** $p<0.001$, using a one-
669 way ANOVA and post hoc Tukey test.

670

671 **Figure 2: cGAS-STING pathway inactivation attenuates DNA damage response.** **a**,
672 representative immunofluorescence images of DNA damage. **b**, quantification of DNA damage in
673 skin ($n_{WT}=6$, $n_{tert-/-}=6$, $n_{sting-/-}=6$, $tert-/-\ sting-/-=6$; WT vs $tert-/-$ $p<0.001$, $sting-/-$ vs $tert-/-$ $p<0.001$, WT
674 vs $tert-/-\ sting-/-$ $p<0.001$, $sting-/-$ vs $tert-/-\ sting-/-$ $p<0.001$). **c**, quantification of DNA damage in
675 testis ($n_{WT}=6$, $n_{tert-/-}=6$, $n_{sting-/-}=6$, $tert-/-\ sting-/-=6$, $N=5-6$, WT vs $tert-/-$ $p<0.001$, $sting-/-$ vs $tert-/-$ $p<$
676 0.001 , WT vs $tert-/-\ sting-/-$ $p<0.001$, $sting-/-$ vs $tert-/-\ sting-/-$ $p<0.001$). **d**, quantification of DNA
677 damage in kidney marrow ($n_{WT}=6$, $n_{tert-/-}=6$, $n_{sting-/-}=6$, $tert-/-\ sting-/-=6$; WT vs $tert-/-$ $p<0.001$, $sting-/-$ vs
678 $tert-/-$ $p<0.001$, WT vs $tert-/-\ sting-/-$ $p<0.001$, $sting-/-$ vs $tert-/-\ sting-/-$ $p<0.001$). **e**, quantification
679 of DNA damage in intestine ($n_{WT}=5$, $n_{tert-/-}=5$, $n_{sting-/-}=5$, $tert-/-\ sting-/-=5$; WT vs $tert-/-$ $p=0.006$, $sting-/-$
680 vs $tert-/-$ $p=0.008$, WT vs $tert-/-\ sting-/-$ $p=0.007$, $sting-/-$ vs $tert-/-\ sting-/-$ $p<0.001$). **f**,
681 representative western blot images of p53. **g**, quantification of p53 levels in the skin ($n_{WT}=4$, $n_{tert-/-}$
682 $=4$, $n_{sting-/-}=4$, $tert-/-\ sting-/-=4$, WT vs $tert-/-$ $p<0.001$, $sting-/-$ vs $tert-/-$ $p<0.001$, $tert-/-$ vs $tert-/-\ sting-/-$
683 $p<0.001$). **h**, quantification of p53 levels in the testis ($n_{WT}=4$, $n_{tert-/-}=4$, $n_{sting-/-}=4$, $tert-/-\ sting-/-=4$, WT vs
684 $tert-/-$ $p=0.050$, $tert-/-$ vs $tert-/-\ sting-/-$ $p=0.048$). **i**, quantification of p53 levels in the kidney marrow
685 ($n_{WT}=4$, $n_{tert-/-}=4$, $n_{sting-/-}=4$, $tert-/-\ sting-/-=4$, $sting-/-$ vs $tert-/-$ $p=0.017$, $tert-/-$ vs $tert-/-\ sting-/-$ $p=0.022$).
686 **j**, quantification of p53 levels in the intestine ($n_{WT}=5$, $n_{tert-/-}=5$, $n_{sting-/-}=5$, $tert-/-\ sting-/-=5$, WT vs $tert-/-$
687 $p<0.001$, $sting-/-$ vs $tert-/-$ $p=0.006$, $tert-/-$ vs $tert-/-\ sting-/-$ $p=0.006$). Data are presented as the
688 mean \pm s.e.m.; * $p<0.05$; ** $p<0.01$, *** $p<0.001$, using a one-way ANOVA and post hoc Tukey test.

689

690 **Figure 3: SASP induced by short telomeres are controlled by cGAS-STING pathway.** **a**,
691 representative images of senescence associated beta galactosidase staining in skin, testis, kidney
692 marrow and intestine ($n_{WT}=3$, $n_{tert-/-}=3$, $n_{sting-/-}=3$, $tert-/-\ sting-/-=3$). **b**, RT-qPCR analysis of inflammatory
693 markers and SASP factors in the skin ($n_{WT}=4-8$, $n_{tert-/-}=5-8$, $n_{sting-/-}=6-7$, $tert-/-\ sting-/-=5-7$; *cdkn2a/b*: WT
694 vs $tert-/-$ $p=0.0001$, $sting-/-$ vs $tert-/-$ $p<0.0001$, $tert-/-$ vs $tert-/-\ sting-/-$ $p=0.004$; *cdnk1a*: WT vs
695 $tert-/-$ $p=0.025$, $sting-/-$ vs $tert-/-$ $p=0.014$, $tert-/-$ vs $tert-/-\ sting-/-$ $p=0.013$; *il1b*: WT vs $tert-/-$

696 $p=0.023$, *sting*^{-/-} vs *tert*^{-/-} $p=0.031$, *tert*^{-/-} vs *tert*^{-/-} *sting*^{-/-} $p=0.004$; *tgf1b*: *sting*^{-/-} vs *tert*^{-/-}
697 $p=0.014$, *tert*^{-/-} vs *tert*^{-/-} *sting*^{-/-} $p=0.017$; *mmp15a*: *sting*^{-/-} vs *tert*^{-/-} $p=0.011$, *tert*^{-/-} vs *tert*^{-/-} *sting*^{-/-}
698 $p=0.009$). **c**, RT-qPCR analysis of inflammatory markers and SASP factors in the testis ($n_{WT}=4$ -
699 7 , $n_{tert^{-/-}}=6$ - 11 , $n_{sting^{-/-}}=5$ - 7 , $tert^{-/-}$ *sting*^{-/-} $=5$ - 8 ; *cdkn2a/b*: WT vs *tert*^{-/-} $p=0.0234$; *cdnk1a*: WT vs *tert*^{-/-}
700 $p=0.013$, *tert*^{-/-} vs *tert*^{-/-} *sting*^{-/-} $p=0.018$; *il1b*: *tert*^{-/-} vs *tert*^{-/-} *sting*^{-/-} $p=0.030$; *tgf1b*: WT vs *tert*^{-/-}
701 $p=0.029$, *sting*^{-/-} vs *tert*^{-/-} $p=0.020$, *tert*^{-/-} vs *tert*^{-/-} *sting*^{-/-} $p=0.043$; *mmp15a*: WT vs *tert*^{-/-}
702 $p=0.004$, *sting*^{-/-} vs *tert*^{-/-} $p=0.016$, *tert*^{-/-} vs *tert*^{-/-} *sting*^{-/-} $p=0.028$). **d**, RT-qPCR analysis of
703 inflammatory markers and SASP factors in the kidney marrow ($n_{WT}=5$ - 9 , $n_{tert^{-/-}}=5$ - 11 , $n_{sting^{-/-}}=6$ - 11 ,
704 $tert^{-/-}$ *sting*^{-/-} $=6$ - 10 ; *cdkn2a/b*: WT vs *tert*^{-/-} $p=0.035$, *sting*^{-/-} vs *tert*^{-/-} $p=0.009$, *tert*^{-/-} vs *tert*^{-/-} *sting*^{-/-}
705 $p<0.001$; *cdnk1a*: WT vs *tert*^{-/-} $p=0.002$, *sting*^{-/-} vs *tert*^{-/-} $p=0.001$, *tert*^{-/-} vs *tert*^{-/-} *sting*^{-/-} $p=0.005$;
706 *il1b*: WT vs *tert*^{-/-} $p=0.047$, *sting*^{-/-} vs *tert*^{-/-} $p=0.003$, *tert*^{-/-} vs *tert*^{-/-} *sting*^{-/-} $p=0.014$; *tgf1b*: *sting*^{-/-}
707 vs *tert*^{-/-} $p=0.005$; *mmp15a*: WT vs *tert*^{-/-} $p=0.009$, *sting*^{-/-} vs *tert*^{-/-} $p=0.011$, *tert*^{-/-} vs *tert*^{-/-} *sting*^{-/-}
708 $p=0.008$). **e**, RT-qPCR analysis of inflammatory markers and SASP factors in the intestine ($n_{WT}=5$ -
709 7 , $n_{tert^{-/-}}=5$ - 8 , $n_{sting^{-/-}}=5$ - 6 , $tert^{-/-}$ *sting*^{-/-} $=5$ - 7 ; *cdkn2a/b*: WT vs *tert*^{-/-} $p<0.001$, *sting*^{-/-} vs *tert*^{-/-} $p=0.001$,
710 *tert*^{-/-} vs *tert*^{-/-} *sting*^{-/-} $p=0.038$; *cdnk1a*: WT vs *tert*^{-/-} $p=0.007$, *sting*^{-/-} vs *tert*^{-/-} $p<0.001$, *tert*^{-/-} vs
711 *tert*^{-/-} *sting*^{-/-} $p=0.011$; *il1b*: WT vs *tert*^{-/-} $p=0.004$, *sting*^{-/-} vs *tert*^{-/-} $p=0.012$, *tert*^{-/-} vs *tert*^{-/-} *sting*^{-/-}
712 $p=0.009$; *tgf1b*: WT vs *tert*^{-/-} $p=0.034$, *sting*^{-/-} vs *tert*^{-/-} $p=0.003$; *mmp15a*: WT vs *tert*^{-/-} NS
713 $p=0.060$, *sting*^{-/-} vs *tert*^{-/-} $p=0.021$, *tert*^{-/-} vs *tert*^{-/-} *sting*^{-/-} $p=0.070$). All data are presented as the
714 mean \pm s.e.m.; * $p<0.05$; ** $p<0.01$, *** $p<0.001$, using a one-way ANOVA and post hoc Tukey test
715

716 **Figure 4: cGAS-STING pathway control proliferation in telomeric dysfunction. a**,
717 representative immunofluorescence images of proliferation and apoptosis. **b**, quantification of
718 proliferation in the skin ($n_{WT}=5$, $n_{tert^{-/-}}=6$, $n_{sting^{-/-}}=6$, *tert*^{-/-} *sting*^{-/-} $=6$ WT vs *tert*^{-/-} $p<0.001$, *sting*^{-/-} vs *tert*^{-/-}
719 $p<0.001$, *tert*^{-/-} vs *tert*^{-/-} *sting*^{-/-} $p=0.024$). **c**, quantification of proliferation in the testis ($n_{WT}=6$,
720 $n_{tert^{-/-}}=6$, $n_{sting^{-/-}}=6$, *tert*^{-/-} *sting*^{-/-} $=6$, WT vs *tert*^{-/-} $p<0.001$, *sting*^{-/-} vs *tert*^{-/-} $p<0.001$, *tert*^{-/-} vs *tert*^{-/-}
721 *sting*^{-/-} $p<0.001$). **d**, quantification of proliferation in the kidney marrow ($n_{WT}=8$, $n_{tert^{-/-}}=8$, $n_{sting^{-/-}}=6$,
722 *tert*^{-/-} *sting*^{-/-} $=8$, WT vs *tert*^{-/-} $p=0.002$, *sting*^{-/-} vs *tert*^{-/-} $p=0.004$). **e**, quantification of proliferation in
723 the intestine ($n_{WT}=6$, $n_{tert^{-/-}}=5$, $n_{sting^{-/-}}=6$, *tert*^{-/-} *sting*^{-/-} $=8$). **f**, representative hematoxylin eosin staining of
724 intestine, insets with yellow lines representative of lamina propria thickness **g**, quantification of
725 lamina propria width ($n_{WT}=4$, $n_{tert^{-/-}}=4$, $n_{sting^{-/-}}=4$, *tert*^{-/-} *sting*^{-/-} $=4$, WT vs *tert*^{-/-} $p=0.042$, *sting*^{-/-} vs *tert*^{-/-}
726 $p=0.048$). **h**, representative hematoxylin eosin staining of testis. **i**, quantification of mature sperm
727 area ($n_{WT}=4$, $n_{tert^{-/-}}=4$, $n_{sting^{-/-}}=4$, *tert*^{-/-} *sting*^{-/-} $=4$, WT vs *tert*^{-/-} $p<0.002$, *sting*^{-/-} vs *tert*^{-/-} $p<0.001$, *tert*^{-/-}
728 vs *tert*^{-/-} *sting*^{-/-} $p=0.006$). **l**, RT-qPCR analysis of YAP-TAZ pathway targets in the intestine ($n_{WT}=4$,
729 $n_{tert^{-/-}}=4$, $n_{sting^{-/-}}=5$, *tert*^{-/-} *sting*^{-/-} $=5$, *ctfg*: WT vs *tert*^{-/-} $p=0.016$ *sting*^{-/-} vs *tert*^{-/-} $p=0.005$, *tert*^{-/-} vs *tert*^{-/-}
730 *sting*^{-/-} $p=0.044$; *cyr61*: WT vs *tert*^{-/-} $p=0.030$, *sting*^{-/-} vs *tert*^{-/-} $p=0.023$, *tert*^{-/-} vs *tert*^{-/-} *sting*^{-/-}
731 $p=0.046$). **m**, RT-qPCR analysis of YAP-TAZ pathway targets in the testis ($n_{WT}=7$, $n_{tert^{-/-}}=8$, $n_{sting^{-/-}}=6$ -
732 7 , *tert*^{-/-} *sting*^{-/-} $=7$ - 8 , *ctfg*: *tert*^{-/-} vs *tert*^{-/-} *sting*^{-/-} $p=0.008$, *cyr61*: *tert*^{-/-} vs *tert*^{-/-} *sting*^{-/-} $p=0.011$). All
733 data are presented as the mean \pm s.e.m.; * $p<0.05$; ** $p<0.01$, *** $p<0.001$, using a one-way ANOVA
734 and post hoc Tukey test.
735

736 **Figure 5: cGAS-STING pathway rescues premature aging phenotypes. a**, quantification of
737 male fertile capacity ($n_{WT}=15$, $n_{tert^{-/-}}=10$, $n_{sting^{-/-}}=14$, *tert*^{-/-} *sting*^{-/-} $=13$), WT vs *tert*^{-/-} $p<0.001$, *sting*^{-/-} vs
738 *tert*^{-/-} $p<0.001$, WT vs *tert*^{-/-} *sting*^{-/-} $p=0.011$, *sting*^{-/-} vs *tert*^{-/-} *sting*^{-/-} $p<0.001$, *tert*^{-/-} vs *tert*^{-/-}
739 *sting*^{-/-} $p=0.002$). **b**, representative images of adult zebrafish and quantification of aging
740 phenotypes scored as kyphosis and cachexia ($n_{WT}=10$, $n_{tert^{-/-}}=12$, $n_{sting^{-/-}}=11$, *tert*^{-/-} *sting*^{-/-} $=12$, WT vs
741 *tert*^{-/-} $p<0.001$, *sting*^{-/-} vs *tert*^{-/-} $p<0.001$, WT vs *tert*^{-/-} *sting*^{-/-} $p<0.001$, *sting*^{-/-} vs *tert*^{-/-} *sting*^{-/-}
742 $p=0.003$, *tert*^{-/-} vs *tert*^{-/-} *sting*^{-/-} $p<0.001$). **c**, quantification of weight in adult zebrafish ($n_{WT}=12$,
743 $n_{tert^{-/-}}=13$, $n_{sting^{-/-}}=11$, *tert*^{-/-} *sting*^{-/-} $=13$, WT vs *tert*^{-/-} $p<0.001$, *sting*^{-/-} vs *tert*^{-/-} $p=0.004$, *tert*^{-/-} vs *tert*^{-/-}
744 *sting*^{-/-} $p=0.012$). **d**, quantification of seminoma ($n_{WT}=17$, $n_{tert^{-/-}}=16$, $n_{sting^{-/-}}=21$, *tert*^{-/-} *sting*^{-/-} $=18$, WT vs
745 *tert*^{-/-} $p=0.012$, *sting*^{-/-} vs *tert*^{-/-} $p=0.002$, *tert*^{-/-} vs *tert*^{-/-} *sting*^{-/-} $p=0.027$). **e**, quantification of
746 survival $n_{WT}=24$, $n_{tert^{-/-}}=38$, $n_{sting^{-/-}}=32$, *tert*^{-/-} *sting*^{-/-} $=37$, WT vs *tert*^{-/-} $p=0.008$, *sting*^{-/-} vs *tert*^{-/-}
747 $p<0.001$, *tert*^{-/-} vs *tert*^{-/-} *sting*^{-/-} $p=0.010$). Data are presented as the mean \pm s.e.m. * $p<0.05$;
748 ** $p<0.01$, *** $p<0.001$, using a one-way ANOVA and post hoc Tukey test. Seminoma occurrence
749 and survival data were analyzed using Log-rank tests, ** $p<0.01$, *** $p<0.001$.

Figures and Figure Legends

Figure 1

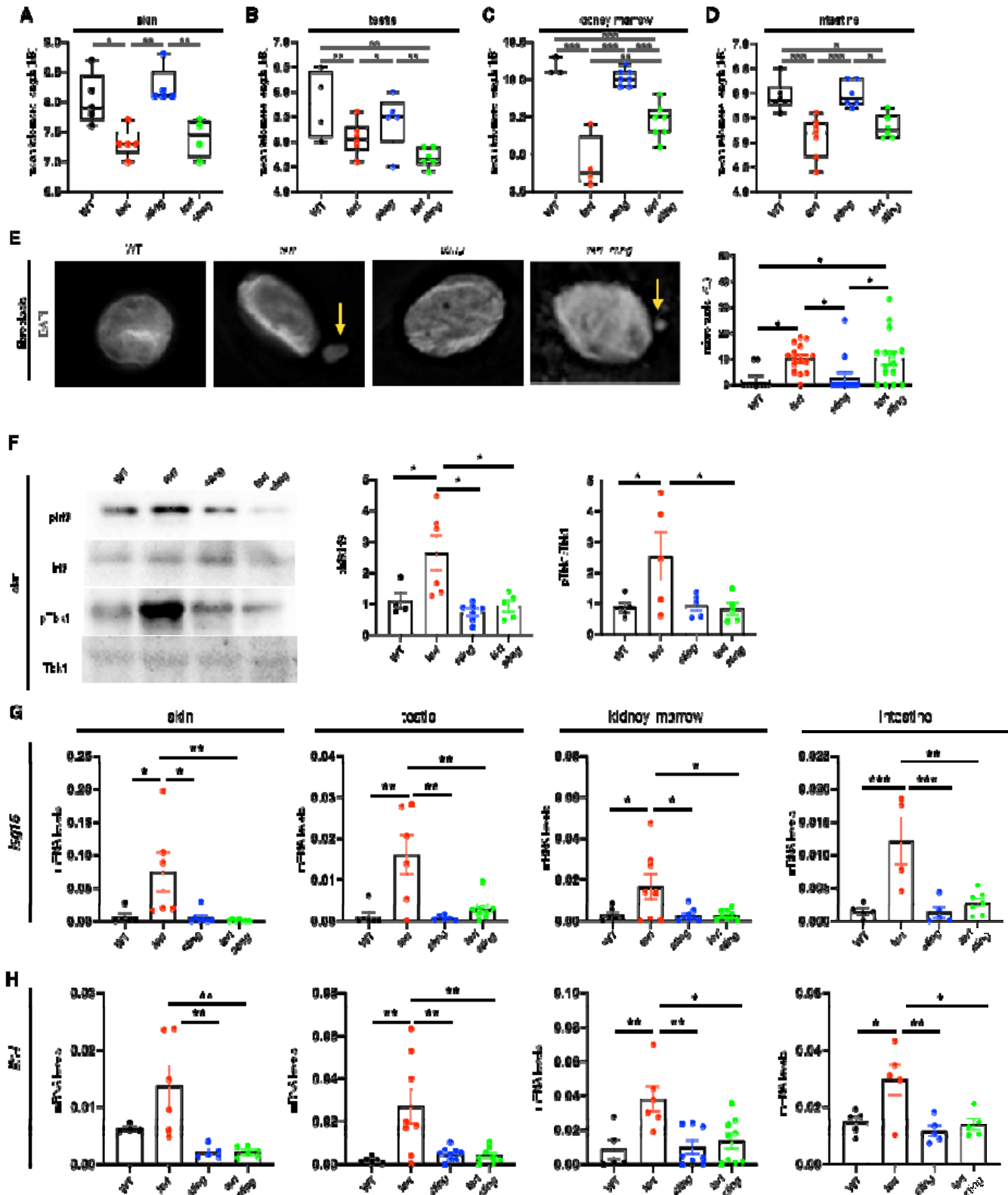


Figure 2

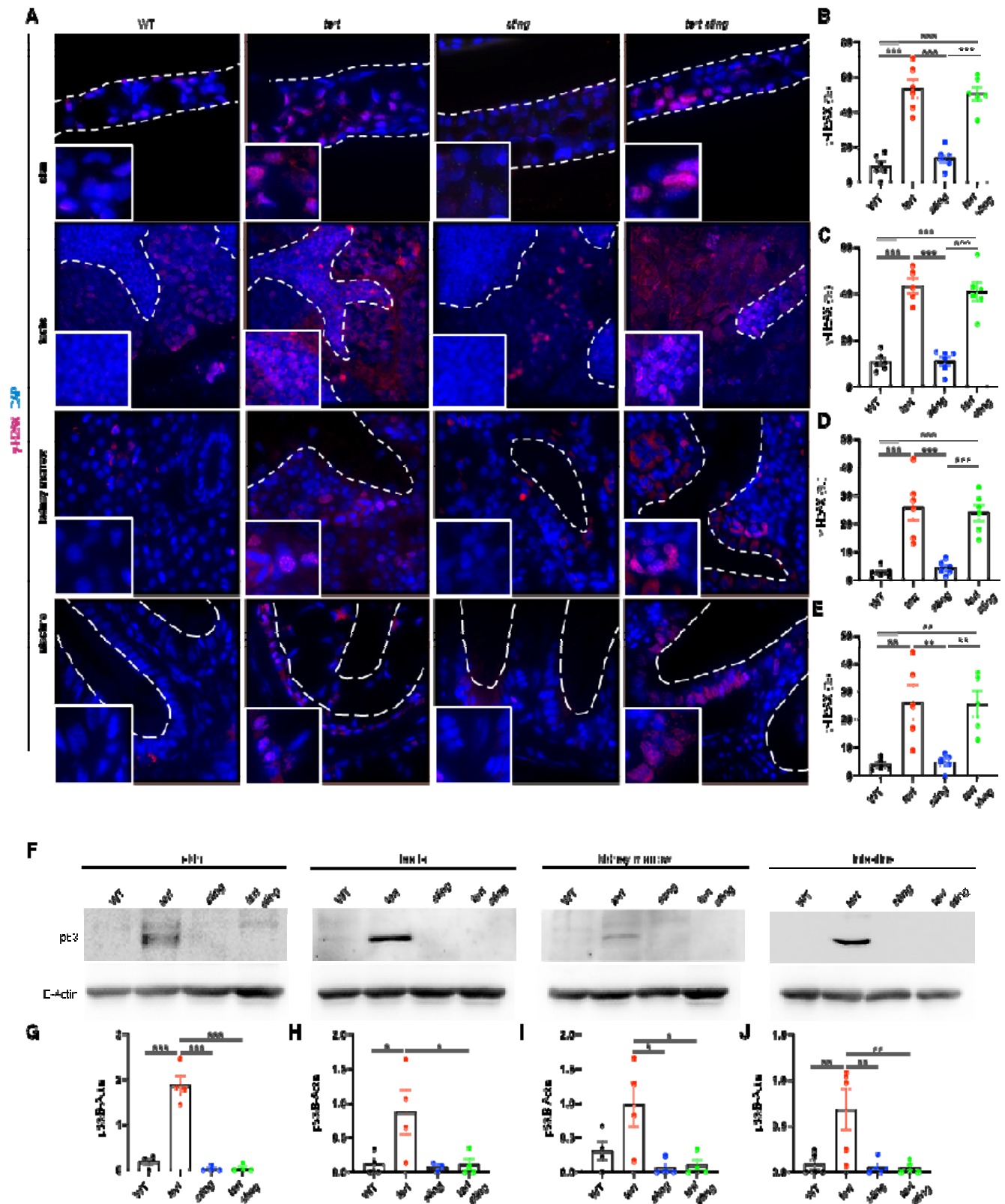


Figure 3

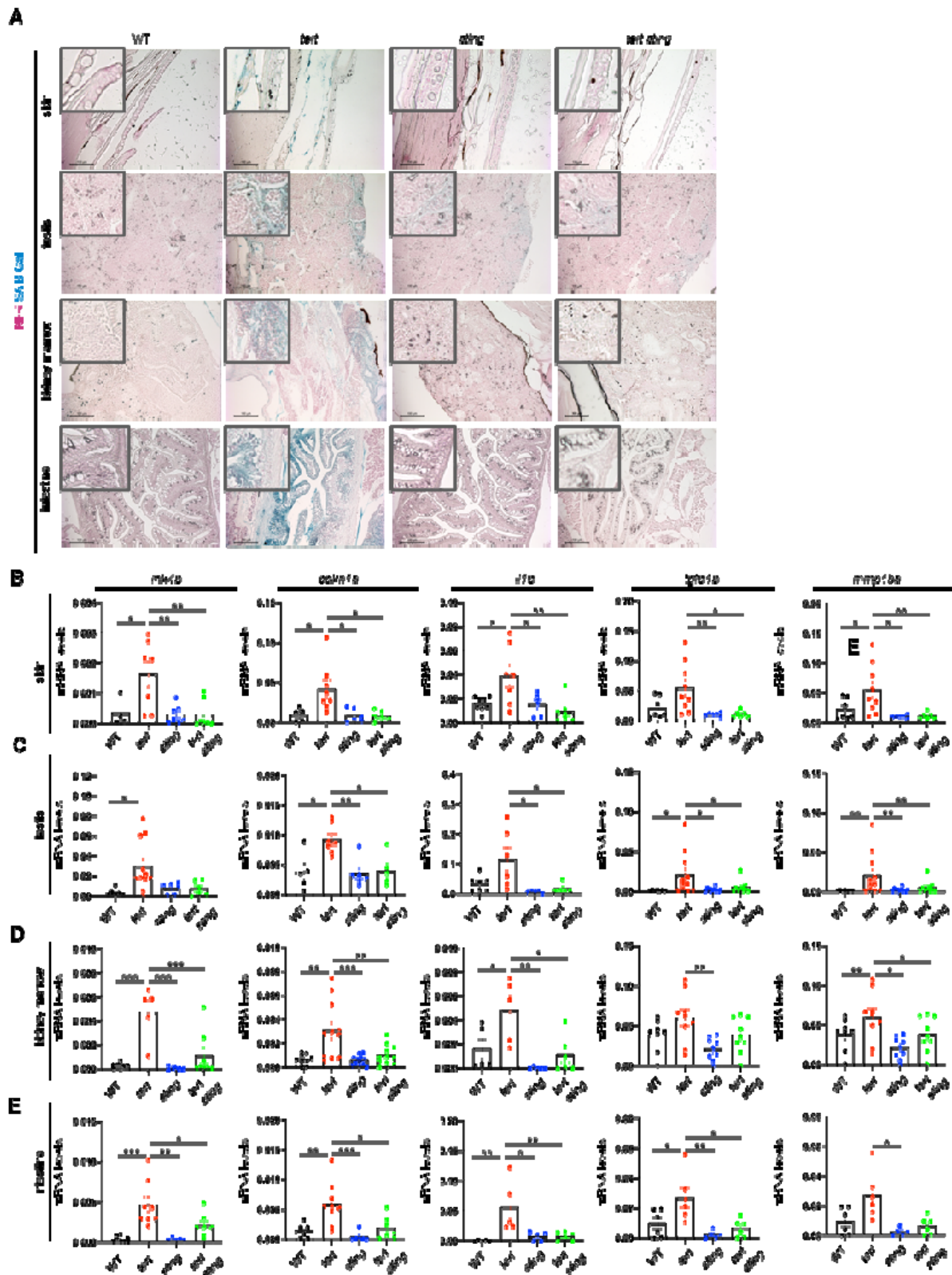


Figure 4

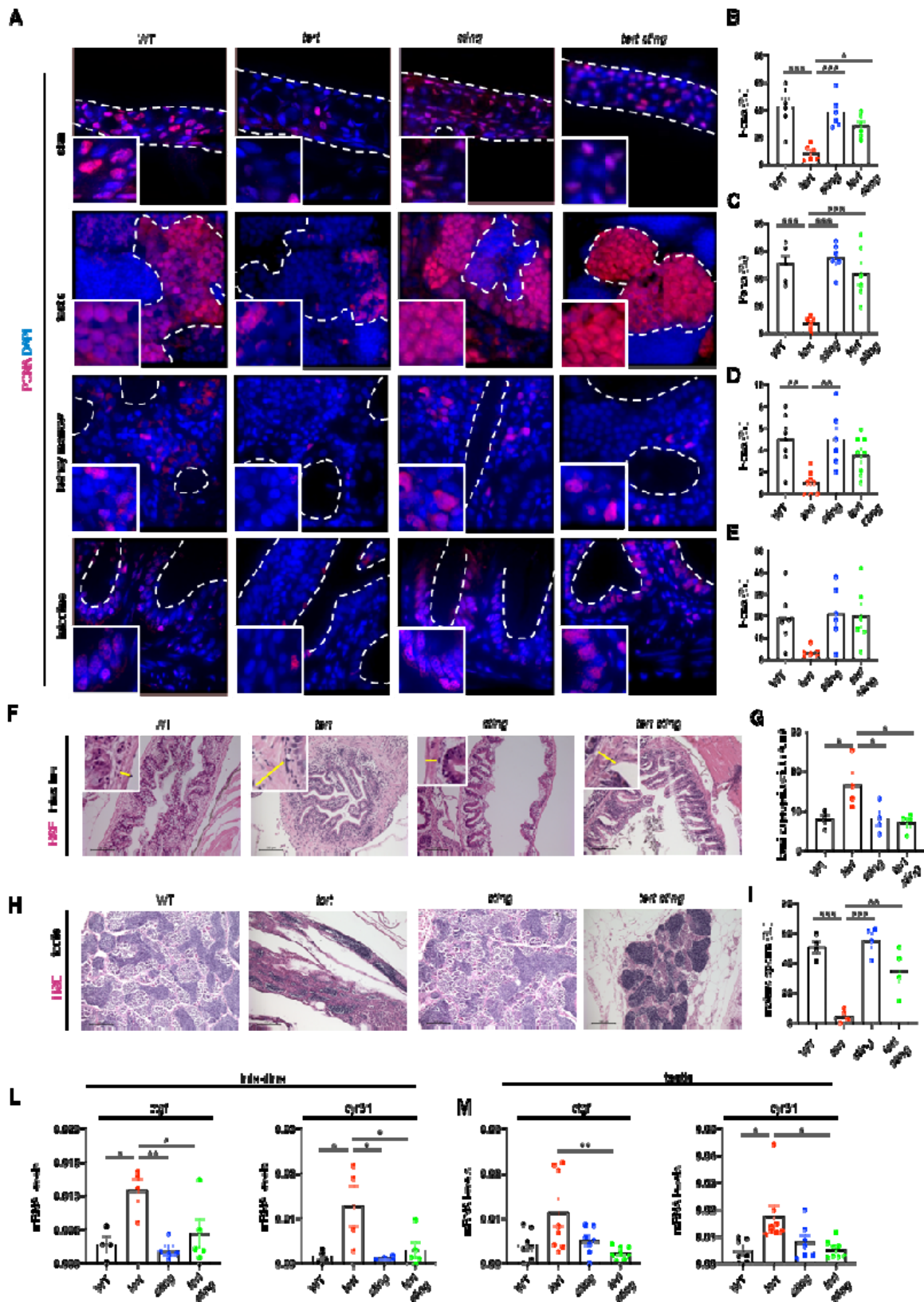


Figure 5

